A Cu/Cu_2O@C composite catalyst derived from wood-chips for the efficient one-pot oxidation of cyclohexane to adipic acid

Wang Sheng[†], Chen Zhijia[†], Wang Xiao, Yuan Chunhua, Li Songbo, Yang Huimin[*]

(*School of Chemistry and Chemical Engineering*, *Inner Mongolia University of Science & Technology*, *Baotou* 014010, *China*)

Abstract: Adipic acid is widely used in fine chemical synthesis, biomedicine and other industrial fields, and is a key monomer for the synthesis of nylon-6,6 and nylon-6. Industrially, it is produced by the efficient catalytic oxidation of cyclohexane. However, the activation of the inert C—H bonds in cyclohexane remains a major challenge in the highly selective synthesis of acid products. Using a composite catalyst of copper on a carbon support produced from wood chip biomass, a green catalytic system was established for the one-pot oxidative synthesis of adipic acid from cyclohexane. Wood chips has two functions during pyrolysis: it acts as a carbon support precursor and an in-situ reducing agent, which reduces Cu^{2+} into Cu/Cu_2O active species to obtain Cu/Cu_2O@C composite catalysts. The abundant defects in biomass carbon form strong coordination interactions with the copper active components, which effectively regulate the electronic distribution of active sites and improve the catalytic performance. Under optimized conditions (100 °C, 12 h), the Cu/Cu_2O@C-0.1 catalyst achieves a cyclohexane conversion of 19.36% and an adipic acid selectivity of 73.28%. Mechanistic investigations show that the electronic interaction between the biomass carbon support and the copper species strengthens the adsorption of cyclohexanone, which is critical for promoting the selective formation of adipic acid. This study provides a viable strategy for developing eco-friendly, low-cost and high-efficiency advanced catalytic materials.

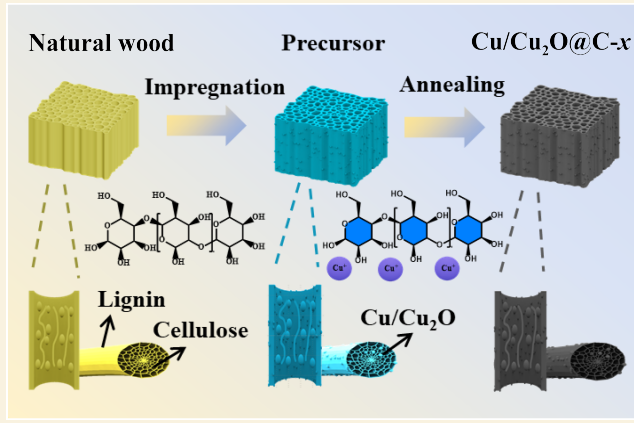

Key words: Cyclohexane oxidation；Adipic acid；Wood chips；Biomass carbon；Cu/Cu_2O active species

1 Introduction

The aerobic oxidation of saturated C—H bonds under mild conditions represents a considerable challenge in chemical synthesis[1]. In particular, the oxidation of cyclohexane to produce KA oil (a mixture of cyclohexanone and cyclohexanol) and adipic acid (AA) carries significant industrial relevance, as AA is a key monomer for the synthesis of nylon-6,6 and nylon-6, both widely employed in engineering plastics and synthetic fibers[2]. Currently, industrial AA production mainly relies on the nitric acid oxidation route, in which cyclohexane is first oxidized by air or H_2O_2 to form KA oil, followed by further oxidation of KA oil to AA using nitric acid. Despite a near-complete conversion of KA oil with 93%−95% selectivity to AA, this process suffers from several serious drawbacks, including high energy consumption, harsh operating conditions, and substantial emissions of N_2O, which conflicts with the principles of green and low-carbon chemistry[3–5].

To address these challenges, extensive research efforts are invested in the development of environmentally friendly catalytic systems capable of oxidizing cyclohexane under mild conditions. Various catalysts, such as Au-TiO_2, VPO-CeO_2, Au-GOS, AuPd/TiO_2, and Mn/HTS-1, have been reported to enhance the efficiency of adipic acid synthesis while re-

Received: March 04, 2026
Revised: May 19, 2026
Accepted: May 21, 2026

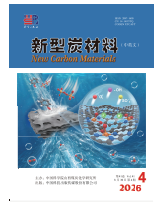

ducing nitrous oxide emissions[6–8]. However, these systems often rely on environmentally unfriendly strong oxidants, such as tert-butyl hydroperoxide (TBHP), or require noble metal catalysts, which limits their potential for large-scale industrial applications[9]. In this context, copper-based catalysts have shown significant promise due to their flexible redox chemistry and ability to stabilize multiple oxidation states during reaction conditions, making them effective for C—H bond activation and selective oxidation processes[10–11]. Liu et al. developed a stable Cu-based core-shell catalyst by a facile synthesis. The copper nanoparticles (Cu NPs) and copper oxides (Cu_xO_y) within the structure promote C—H activation in benzyl alcohol, enabling efficient oxidation to benzoic acid[12]. Researchers synthesized a catalyst composed of copper nanoparticles supported on amorphous carbon nitride through a simple and environmentally friendly method. The copper nanoparticles in this catalyst effectively promote the activation of C—H bonds in cyclohexane, achieving a 25.5% conversion rate with 55% selectivity for adipic acid[13]. Particularly noteworthy are the Cu/Cu_2O composites, which feature synergistic interactions between metallic Cu and Cu_2O phases that promote oxygen activation and enhance the selective transformation of reaction intermediates[14]. Nevertheless, it remains challenging to design catalysts with high dispersion, stability of copper active sites, and strong metal-support interactions.

In recent decades, biomass-derived carbon materials have emerged as highly attractive candidates due to their excellent sustainability, tunable porosity, and rich surface functionalities. The inherent oxygen-containing groups and structural defects in such carbon materials can reduce the hydrophobicity of the support surface, which facilitates the anchoring and stabilization of metal or metal oxide nanoparticles, while also modulating their electronic environment through metal-support interactions. Among all biomass-derived carbon materials, wood-derived ones possess unique structural advantages. Their natural hierarchical pore systems create ideal confined spaces for metal nanoparticle loading. Simultaneously, their abundant intrinsic defects enhance the adsorption and activation of key reaction intermediates through defect engineering. Previous studies have shown that structure-function integrated supported catalysts can be constructed by selecting biomass precursors and tuning pyrolysis processes[15]. Examples include Bougainvillea glabra-derived Cu_2O/BGC, cyanobacterial biomass-derived HTCC, and sunflower straw-based CuPc@C systems, all of which have demonstrated enhanced catalytic performance in reactions such as the selective oxidation of cyclohexane[16–18]. However, existing biomass carbon-supported catalysts still face several key challenges. Under practical oxidation reaction conditions, metal active centers are prone to migration and aggregation during thermo-catalytic processes. Hierarchical pore structures may collapse during prolonged reactions, and the inherent oxidation resistance of the carbon support remains inadequate[19]. These issues not only limit the utilization of active sites but also lead to insufficient catalytic cycling stability, thereby constraining their industrial application potential[20]. For the industrially significant reaction of mild cyclohexane oxidation to adipic acid, systematic studies on wood-derived carbon-supported Cu/Cu_2O composite catalysts are still lacking. This gap in research is particularly evident in the mechanistic understanding of the synergistic effect between the Cu/Cu_2O structure and the carbon support and its impact on catalytic performance, adsorption orientation, and reaction pathways[21]. Therefore, this study aims to construct structurally stable wood-derived carbon-supported Cu/Cu_2O composites through controlled preparation methods, elucidate the synergistic effect between the Cu/Cu_2O structure and the carbon support in enhancing catalytic performance, and provide theoretical foundations and material insights on the development of efficient and stable biomass carbon-based oxidation catalysts[22].

Herein, we reported a facile and sustainable synthesis strategy for a wood chip-derived Cu-based composite catalyst through one-step in-situ pyrolysis. In this approach, wood chips serve simultaneously as a carbon precursor, a structural template, and an in-situ reducing agent, enabling the controlled formation

of highly dispersed Cu/Cu_2O nanoparticles embedded within a porous carbon matrix. The resulting catalyst exhibits excellent activity and selectivity in the one-pot oxidation of cyclohexane to adipic acid under mild conditions. Through the combination of spectroscopic characterization and mechanistic studies, we demonstrate that the interaction between Cu/Cu_2O and the carbon support alters the chemical state of the material. Meanwhile, the defect in the carbon support facilitates the recombination of Cu-based catalyst. The synergistic effect between Cu/Cu_2O and the carbon support plays a critical role in enhancing structural stability and optimizing the electronic structure of active sites, thereby enhancing the adsorption and conversion of key intermediates such as cyclohexanone. This work not only provides an efficient and eco-friendly catalytic system for adipic acid production but also offers deeper insights into the design of biomass-supported metal catalysts for sustainable oxidation chemistry.

2 Experiment

2.1 Chemicals and materials

Wood chips were collected from timber processing plants in Baotou, China. Prior to the experiment, they underwent a series of pretreatments. First, they were thoroughly rinsed with deionized (DI) water to remove surface impurities. They were then immersed in 1 mol L^{-1} HCl for 24 h to dissolve inorganic elements. Finally, the treated chips were washed repeatedly with DI water until a neutral pH was reached, and subsequently oven-dried at 80 °C for 12 h.

All chemical reagents were of analytical grade and used without further purification. Specifically, copper nitrate trihydrate ($Cu(NO_3)_2·3H_2O$, ≥99%) was obtained from Sinopharm Group Chemical Reagent Co., Ltd. Hydrogen peroxide (H_2O_2, 30% in water) was purchased from Tianjin Damao Chemical Reagent Factory, China. Cyclohexane (≥99%) and all other reagents were supplied by Shanghai Aladdin Biochemical Technology Co., Ltd.

2.2 Synthesis of Cu/Cu_2O@C-*x* catalysts

The Cu/Cu_2O@C-*x* catalysts were synthesized through an in-situ pyrolysis method. Typically, 1.0 g of wood chips was immersed in 100 mL of an aqueous $Cu(NO_3)_2·3H_2O$ solution with concentrations of *x* mol L^{-1} (*x*=0.05, 0.1, 0.2 and 0.4). After sonication for 3 h, the samples were washed with DI water until neutral pH was achieved and then dried overnight at 80 °C. The dried precursor was subsequently carbonized at 1000 °C for 8 h under N_2 atmosphere with a heating rate of 5.0 °C min^{-1}. The resulting catalysts were named as Cu/Cu_2O@C-*x*. A metal-free wood-derived carbon material was prepared under identical conditions with the sole exception of copper salt and labeled as C-0. For comparison, two additional catalysts (Cu/C-0.1-I and Cu/C-0.1-M) were prepared using impregnation (24 h immersion time) and mechanical mixing (blending equal masses of solid copper nitrate and wood chips) methods, respectively, while maintaining all other preparation steps consistent.

2.3 Characterizations

X-ray diffraction (XRD) patterns were obtained on a Smartlab-SE with Cu *K*α radiation operating at 40 kV and 100 mA with a scanning rate of 20 °/min. Fourier-transform infrared spectroscopy (FT-IR) analysis was performed using a NEXUS spectrometer over the range of 4000-500 cm^{-1}. X-ray Photoelectron Spectra (XPS) was operated on the ESCALAB 250Xi spectrometer with Al *K*α radiation, and the C 1s standard peak of 284.8 eV was used for calibration. Electron paramagnetic resonance (EPR) signal was collected using a Bruker A300-10/12 spectrometer. The morphology of catalysts was observed by scanning electron microscopy (SEM, SU8020). Transmission electron microscopy (TEM) measurements and energy dispersive X-rays spectroscopy (EDX) were carried out on a Titan ETEM G2 80-300 (FEI Co., USA) with an accelerating voltage of 300 kV. N_2 adsorption and desorption of catalysts were analyzed with an ASAP 2420 (Micromeritics Co., USA) at 77 K. Raman measurements were performed on a Lab RAM HR Evolution spectrometer (HORIBA Instruments Inc., Japan) using a 532 nm He/Ne laser source. The Cu loading in the samples was determined by inductively coupled plasma optical emission spectrometry (Thermo Fisher iCAP 7400). The mass change of the

materials during heating was tested using a simultaneous thermal analyzer (STA 2500 Regulus) to determine their thermal stability and composition. The elemental content of the wood chip carrier was determined using an elemental analyzer (Elementar Vario Micro Cube).

2.4 Cyclohexane oxidation

A typical reaction condition can be set up by adding 1 mmol cyclohexane, 4 mmol H_2O_2 (30%) and 10 mg catalyst to a glass tube which was heated to 100 °C for 12 h while stirring at 800 r min^{-1}. After the reaction finished, 6 mL of ethyl acetate (EtOAc) was added into the tube. Gas chromatography (GC) was carried out using a flame ionization detector and KB-5 capillary column. Conversion of cyclohexane and the selectivity for KA oil using biphenyl were measured and compared. In addition, adipic acid and by-products were qualitatively analyzed by liquid chromatography-mass spectrometry. The content of adipic acid was determined by titration with 0.1 mol L^{-1} NaOH aqueous solution. The conversion of cyclohexane (X_{conv}, %) and selectivity (S, %) were calculated as follows.

$$X_{conv} = \frac{n_{CHA}}{n_0} \times 100\% \quad (1)$$

$$S = \frac{n_{AA}}{n_{CHA}} \times 100\% \quad (2)$$

here, n_0 represents the initial amount of cyclohexane (mol), while n_{CHA} and n_{AA} correspond to the amount of cyclohexane consumed (mol) and the amount of product (mol) at the end of the reaction, respectively.

To evaluate the catalyst stability, the spent catalyst was recycled from the reaction solution by filtration, washed with ethanol, and dried at 80 °C for 12 h. Then, it was used in the next run of the cycle experiment. The total selectivity equals the combined selectivity for adipic acid (AA), cyclohexanone (K), cyclohexanol (A), and other products.

3 Result and discussion

3.1 Catalyst characterization analysis

The steps of synthesis for Cu/Cu_2O@C-x are shown in Fig. 1a. Initially, copper ions were loaded onto the wood chips by ultrasonic impregnation to obtain the Cu-based carbon precursor. The copper-loaded precursor was then carbonized in a tube furnace under a N_2 atmosphere. During the heating process, the resulting carbon reduced Cu^{2+} to Cu^+ and Cu^0, ultimately forming the Cu/Cu_2O@C composite[23]. The copper loading in different samples, as determined by ICP-OES, is 15.5%, 27.9% and 82.3% for Cu/Cu_2O@C-0.05, Cu/Cu_2O@C-0.1 and Cu/Cu_2O@C-0.4, respectively.

The SEM results show that the C-0 catalyst exhibits a lotus root-like pore structure, which is attributed to the intrinsic structure of the wood chips that remained intact after calcination (Fig. S1a). The rich pore structure provides ample sites for metal loading. After copper loading, the surface of the wood chip carbon becomes rough (Fig. 1b, c and Fig. S1b-d). This roughness is likely due to the carbon on the surface of the carrier participating in the reduction of Cu^{2+} during the carbonization process, with the roughness increasing as the Cu^{2+} concentration rises[24]. Notably, the copper morphology in Cu/Cu_2O@C-0.1 is uniformly sized and evenly dispersed within the pore channels of the carrier. As the Cu^{2+} concentration continued to increase, especially in Cu/Cu_2O@C-0.4, the number of copper particles distributed within the pores and on the surface increases significantly, leading to agglomeration and inhomogeneity in the metal particle distribution[25]. The results demonstrate that at an optimal concentration, copper ions form a flocculent catalyst where the species are uniformly distributed and firmly anchored onto the carbon surface, indicating strong interactions with the carbon carrier that enhance the catalyst's stability during the reaction[26].

TEM results are shown in Fig. 1d, in which the catalyst surface is seen decorated with well-dispersed metal nanoparticles and clusters. High-resolution imaging (Fig. 1e and e1-e3) reveals distinct lattice fringes with interplanar spacings of 0.249 and 0.212 nm, corresponding to the (111) crystal planes of Cu_2O and of Cu, respectively. Furthermore, energy-dispersive X-ray spectroscopy (EDS) mapping (Fig. 1f) confirms the uniform distribution of C, O and Cu throughout

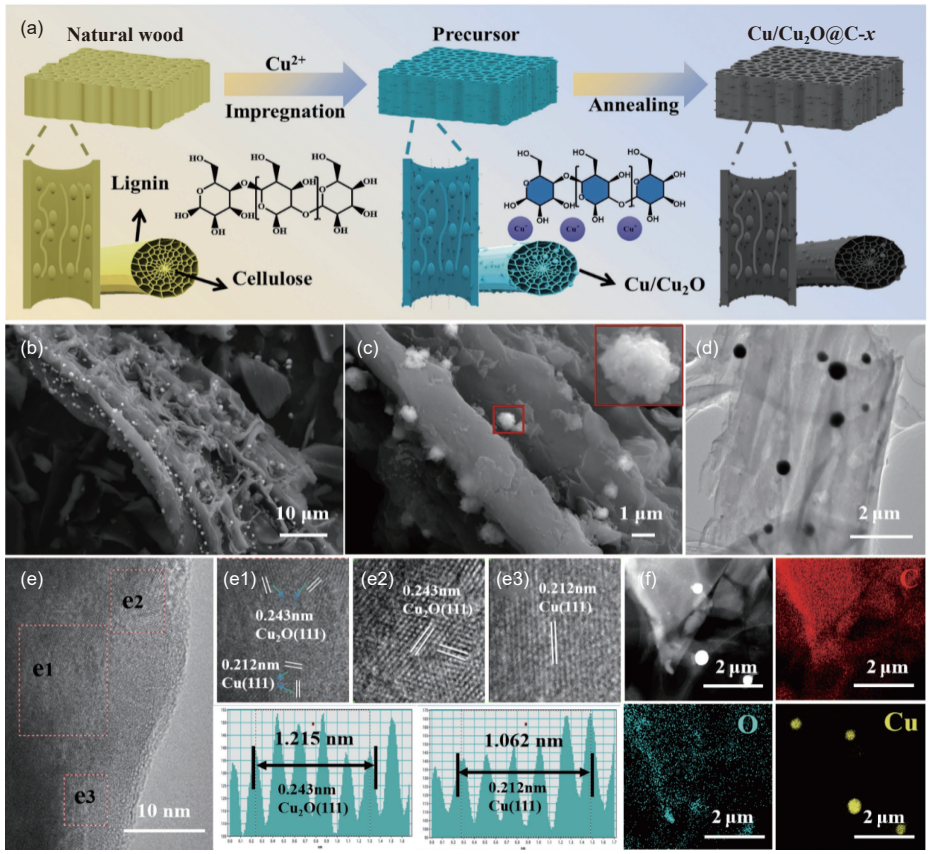

Fig. 1　(a) The schematic of synthesis steps of Cu/Cu_2O@C-*x* catalysts. (b, c) SEM and (d, e) TEM images of Cu/Cu_2O@C-0.1 materials. (e1-e3) The lattice planes and spacings in the catalyst. (f) EDX images of Cu/Cu_2O@C-0.1

the material[27]. Notably, the Cu nanoparticles are found to be tightly embedded within the carbon matrix, indicating a strong interaction between the metal species and the biomass-derived carbon support. EDX analysis on the SEM images of the Cu/Cu_2O@C-0.1 material (Fig. S2) aligns with the aforementioned conclusion.

Fig. 2a shows the XRD patterns of C-0 and Cu/Cu_2O@C-*x* (*x*=0.05, 0.1, 0.4). C-0 exhibits characteristic diffraction peaks at 26°, 44° and 54°, which correspond to the (002), (101) and (004) crystal planes of graphite, respectively. Additionally, there is a broad peak at 22° which is primarily attributed to the amorphous carbon phase. These observations suggest that partial graphitization occurred during the carbonization of the wood chips. In the XRD pattern of Cu/Cu_2O@C-*x*, diffraction peaks centered at 43°, 50° and 74° correspond to the (111), (200) and (220) planes of Cu, respectively. Furthermore, distinct peaks at 36.4°, 42.3° and 61.5° are observed, which are attributed to the (111), (200) and (220) planes of Cu_2O, respectively[28]. It is shown that a portion of Cu^{2+} species is reduced to Cu^0 during the carbonization process, with the remainder forming Cu_2O, ultimately yielding Cu/Cu_2O microparticles[29]. Moreover, the intensity of the graphitic-like carbon peaks in the catalysts decreases as metal loading increases, which may be attributed to the higher copper content. The intensity of the Cu diffraction peaks first increases and then decreases with the rise of Cu^{2+} concentration. Notably, the Cu/Cu_2O@C-0.1 sample exhibits the weakest Cu diffraction peak, indicating the lowest crystallinity of the reduced copper among all samples[30]. This phenomenon likely arises from the strong interaction between the copper species and the carbon support, which aligns with the flocculent morphology observed in SEM images. Further insights on the surface structure of the prepared samples were obtained from the Raman spectra (Fig. 2b). The distinct bands located at 1339 and 1592 cm^{-1} correspond to the *D*

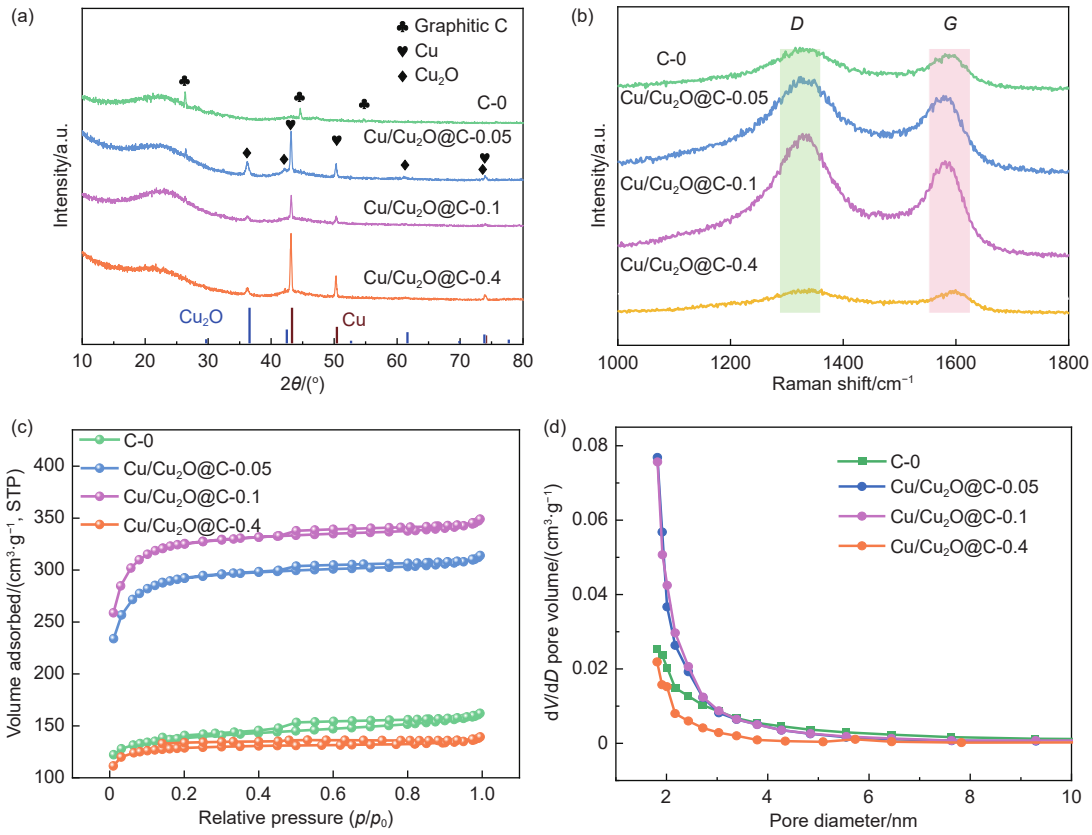

Fig. 2 (a) XRD patterns, (b) Raman spectra, (c) N_2 sorption isotherms and (d) Pore size distribution of C-0 and Cu/Cu_2O@C-*x* catalysts

band (sp^3-hybridized carbon) and *G* band (in-plane vibration of sp^2-hybridized carbon), respectively. The intensity ratio (I_D/I_G) reflects the degree of structural disorder and defect density in the carbon framework. During the pyrolysis process, small organic molecules in the biomass condense into conjugated aromatic rings, generating a considerable number of defect sites along the biochar boundaries[31]. The I_D/I_G ratios of Cu/Cu_2O@C-0.05 (1.23) and Cu/Cu_2O@C-0.1 (1.30) are notably higher than that of C-0 (1.08), indicating that the introduction of Cu $(NO_3)_2$ promotes the formation of additional structural defects during carbonization. In contrast, the I_D/I_G ratio of Cu/Cu_2O@C-0.4 (1.07) is comparable to that of C-0, and the overall intensities of the *D* and *G* bands are lower[32]. This suggests that excessive Cu precursor concentration hinders the formation of aromatic ring structures and defect generation. These observations are consistent with the XRD results.

The N_2 adsorption-desorption isotherms and pore size distributions of the samples are presented in Fig. 2c and 2d. All catalysts exhibit characteristic type IV isotherms with distinct hysteresis loops in the 0.4−1.0 p/p_0 range, confirming their mesoporous structures (Fig. 2c). As summarized in Table S1, the textural properties show a strong dependence on Cu-loading. Increasing the Cu^{2+} concentration from 0 to 0.1 mol L^{-1} significantly enhances both the pore volume (0.17−0.4 cm^3 g^{-1}) and BET surface area (546−1268 m^2 g^{-1}). This improvement suggests that copper species promote the development of hierarchical porosity in the lignocellulose-derived carbon matrix, which in turn supports the uniform dispersion of metallic nanoparticles. However, at excessive Cu^{2+} loading (0.4 mol L^{-1}), both surface area (518 m^2 g^{-1}) and pore volume (0.17 cm^3 g^{-1}) decrease dramatically. Fig. 2d indicates that the pores in the samples are primarily micropores (<2 nm) and small mesopores (2−4 nm). However, at high loading levels, the overall pore volume decreases significantly, suggesting that the excessive metal particles block the original small pores. This deterioration is primarily due to the aggregation of copper nanoparticles into large clusters and pore blockage caused by surface deposition.

These findings highlight the critical importance of controlling copper loading precisely when designing high-performance carbon-supported catalysts. Fig. S5 shows the micropore size distributions of the Cu/Cu_2O@C-*x* catalysts. The micropore volume decreases significantly as Cu loading increases. The FTIR comparative analysis in Fig. S6 indicates that calcination significantly alters the chemical structure and functional group composition of wood chips. The appearance of sharp absorption peaks corresponding to —OH stretching, C—H stretching,—OH/C—OH bending, and C—O—C stretching vibrations after calcination demonstrates the successful introduction of abundant oxygen-containing functional groups. This spectral evolution directly reflects the structural transformation from raw biomass into a carbon-based material rich in oxygen functional groups. The thermogravimetric analysis (TGA) curve in Fig. S7 clearly shows the mass loss of wood chips. A sharp, single-step major decomposition process occurs in the range of 200−400 °C. This significant mass loss stage and the subsequent plateau indicate the formation of a stable carbon-based matrix. Elemental analysis (EA) results (Table S3) show that wood chip biomass is composed of 46.72% C, 6.30% H, 0.24% N, and 41.87% O, with no sulfur (S) detected. This composition is typical of lignocellulosic biomass.

The interface electronic states of C-0 and Cu/Cu_2O@C-*x* were further measured through XPS characterization to demonstrate interface interactions. The survey spectrum (Fig. S3) exhibits 3 distinct peaks at 285 eV (C 1s), 532 eV (O 1s), and 941 eV (Cu 2p), confirming the elemental composition of the hybrid materials. The high-resolution C 1s spectrum (Fig. 3a) was deconvoluted into 4 components corresponding to different chemical environments. The peak at 283.5 eV is typical of Cu—C bonds, indicating metal-support interaction. Peaks at 284.7, 285.8 and 288.5 eV are typical of C—C, C—O—C and O—C=O (carboxyl) bonds. Quantitative XPS analysis in Table S2 reveals that as the Cu loading increased, the concentration of C—O—C bonds rose from 16.7% to 21.9%, while that of C—C bonds decreased from 65.4% to 56.9%, and the content of Cu—C groups increased significantly from 0 to 4.8%. After copper ion loading, part of the C—O—C bonds in the carbon material form C—C and Cu—C bonds, leading to a reduction in defect concentration in the loaded catalyst. Therefore, the presence of defect facilitates the formation of Cu—C bonds, thereby enhancing the stability of the resulting catalyst. The O 1s spectra (Fig. 3b) were deconvoluted into three peaks at 530.2, 531.7 and 533.4 eV, which correspond to the Cu—O (Lattice oxygen O_L), C—O (Defect) and O—C=O (Adsorbed oxygen O_A), respectively. In contrast, the peak observed at 530.2 eV in sample C-0 can be attributed to —OH groups. Results indicate that the carbon material contains abundant defect, while the concentration of defect decreases after metal loading, likely due to the formation of Cu—O bonds (Fig. 3b). FT-IR spectra of Cu/Cu_2O@C-*x* catalysts (Fig. S4) confirmed the presence of Cu—O bonds in the composites. Cu 2p analysis (Fig. 3c) reveals 2 dominant peaks at 931.8 eV ($2p_{3/2}$) and 951.6 eV ($2p_{1/2}$) with a spin-orbit splitting of 19.8 eV, characteristic of Cu^0 species. Simultaneously, the presence of peaks at 932 and 951.8 eV, corresponding to Cu^+, confirms that some Cu^{2+} is not fully reduced during synthesis, consistent with the phase analysis results from XRD. Moreover, shifts in the binding energies of Cu, C and O also indicate strong interactions between Cu/Cu_2O and the carbon support, which may contribute to the enhanced catalytic performance[33]. The Cu LMM XPS spectrum for the Cu/Cu_2O@C-0.1 sample is presented in Fig. S8. Spectral fitting confirms the coexistence of metallic copper (Cu^0) and cuprous oxide (Cu_2O) within the composite. The calculated area ratio of the Cu^0 peak to the Cu^+ peak is approximately 0.5. As shown in Fig. 3d, the EPR signal observed after pyrolysis of the biomass-derived carbon material corresponds to unpaired electrons from radicals and structural defects. ERP signal intensity decreases after copper loading despite the fact that oxygen vacancies may be generated in the formed Cu/Cu_2O. The reduction is mainly attributed to 2 factors. First, during the pyrolysis process, part of Cu(II) gains electrons and is reduced to lower oxidation states, such as Cu(I) or

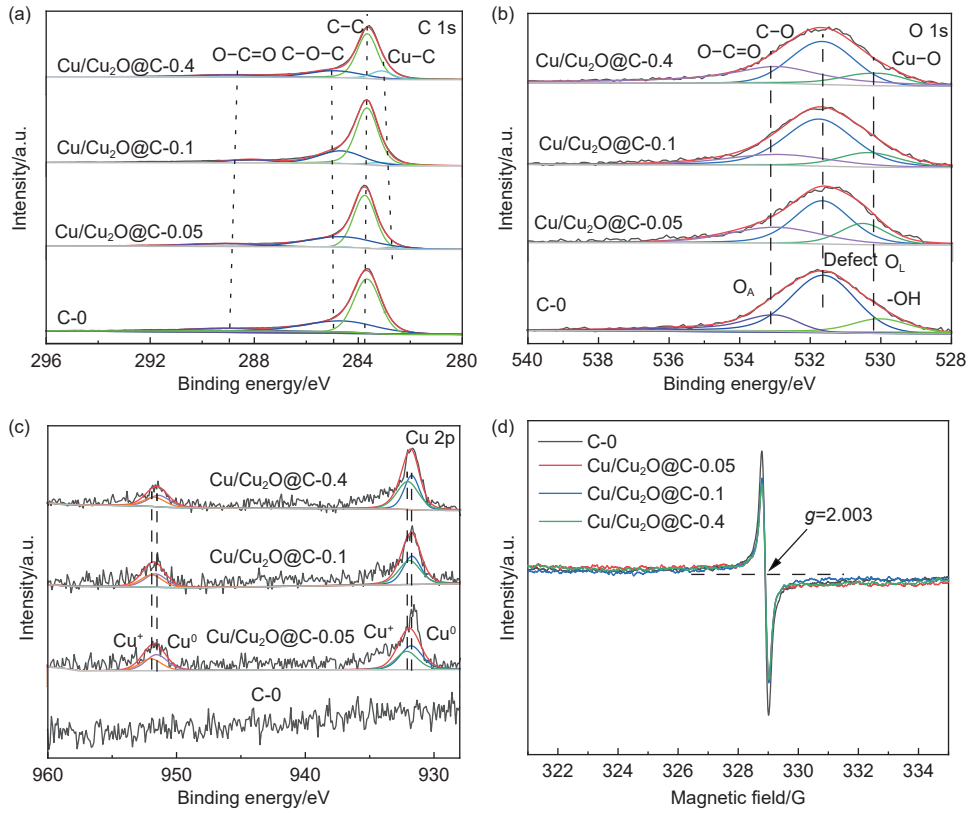

Fig. 3 XPS spectra: (a) C 1s, (b) O 1s and (c) Cu 2p of all Cu/Cu_2O@C-*x* composites. (d) the EPR spectra of C-0 and Cu/Cu_2O@C-0.1

Cu(0), which consumes some unpaired electrons and consequently weakens the EPR signal. Second, the pyrolysis process enhances the interaction between the copper species and the carbon support, likely forming a more stable composite structure. This strong interaction restricts the freedom of the electrons, further reducing the detectable signal from unpaired electrons[34]. After the introduction of copper species, the interaction between copper ions and the carbon support surface formed Cu—C and Cu—O bonds, altering the local chemical structure of the carbon matrix. This strong interaction results in a noticeable decrease in EPR signal, demonstrating enhanced binding between Cu species and the carbon support[35]. Such strengthened metal-support interaction facilitates the uniform dispersion of Cu on the carbon surface and contributes to improved structural stability of the catalyst during catalytic reactions. This conclusion aligns well with the XPS results.

3.2 Catalytic performance

The catalytic performances of C-0 and Cu/Cu_2O@C-*x* were systematically explored through the aerobic oxidation of cyclohexane to AA (Scheme 1). As shown in Table 1, pristine biomass-derived carbon material exhibited negligible catalytic activity, achieving merely 4.3% cyclohexane conversion (Entry 1). The catalytic efficiency demonstrates a distinct copper-loading dependence, reaching optimal performance with Cu/Cu_2O@C-0.1 at 19.3% cyclohexane conversion and 73.28% AA selectivity (Entries 2-3). Such a pronounced enhancement (4.5-fold increase in conversion) unequivocally establishes Cu species as the active sites for the oxidation process. Notably, when the amount of Cu loading is further increased, the selectivity of KA oil shows an increasing trend, but the selectivity of acid decreases to 60% (Entries 4-5). This phenomenon can be attributed to the aggregation of copper nanoparticles, which reduces accessible active sites and prevents deep oxidation. In addition, both the reaction conversion and acid selectivity achieve steady-state values after 12 h of reaction time (Entries 6-7). In control experiments employing alternative synthesis methods, Cu/C-0.1-I and Cu/C-0.1-M yielded inferior conversion rates

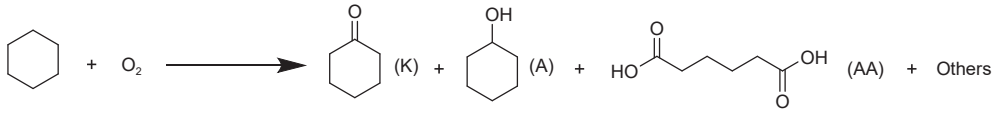

Scheme 1 Cyclohexane oxidation reaction

Table 1 Effect of catalysts on the reaction [a]

Entry	Catalysts	X_{Conv}/%	S_{Total}/%	S_{AA}/%	S_A/%	S_K/%	S_{others}/%
1	C-0	4.29	81.95	58.13	3.75	20.07	18.05
2	Cu/Cu_2O@C-0.05	15.27	79.92	66.09	3.60	10.23	20.08
3	Cu/Cu_2O@C-0.1	19.36	96.68	73.28	14.17	9.23	3.32
4	Cu/Cu_2O@C-0.2	16.05	89.07	63.54	15.87	9.66	10.93
5	Cu/Cu_2O@C-0.4	15.84	86.30	60.00	16.14	10.16	13.70
6[b]	Cu/Cu_2O@C-0.1	11.74	91.52	12.06	50.54	28.92	8.48
7[c]	Cu/Cu_2O@C-0.1	20.51	96.08	75.58	12.83	7.67	3.92
8	Cu/C-0.1-I	11.15	89.81	38.89	29.79	21.14	10.09
9	Cu/C-0.1-M	9.37	75.40	48.35	18.20	8.85	24.60

Note: [a] Reaction conditions: 1 mmol cyclohexane, 10 mg catalyst, 4 mmol H_2O_2, 100 °C, 12 h. [b] 6 h.[c] 24 h.

(11.15% and 9.37%, respectively), though with enhanced KA oil selectivity (25%−60%, Entries 8-9). The comparative results highlight the superiority of our synthesis protocol in creating highly dispersed copper sites. Consequently, Cu/Cu_2O@C-0.1 is identified as the optimal catalyst for subsequent mechanistic investigations.

As shown in Fig. 4a, the dosage of catalyst plays a crucial role in the oxidation performance of cyclohexane. Given that, the reaction conditions can be optimized further by increasing the amount of catalyst from 5 to 10 mg. It is observed that the selectivity of cyclohexanone decreases sharply from 22% to 9.2%, while the selectivity of AA increases significantly from 43.1% to 73.3%. This observation suggests that AA is primarily formed by the over-oxidation of cyc-

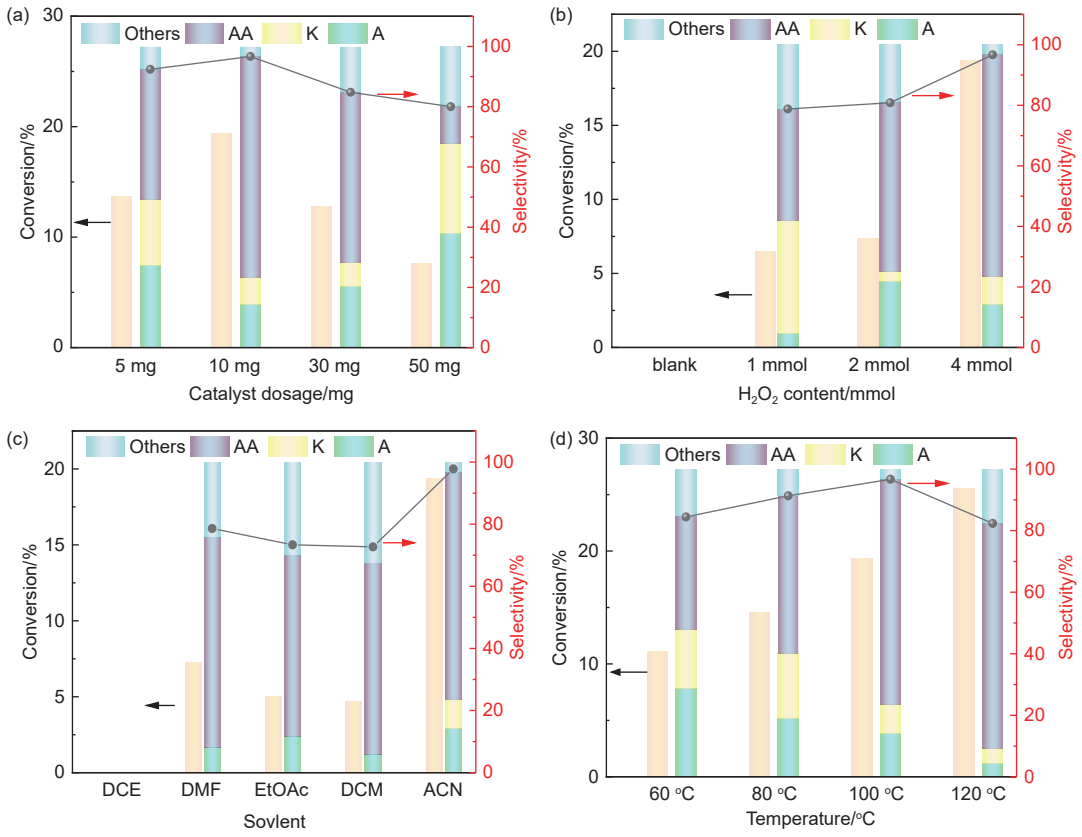

Fig. 4 The effect of (a) catalyst content, (b) H_2O_2 content, (c) solvent and (d) temperature on cyclohexane oxidation performance over Cu/Cu_2O@C-0.1

lohexanone. Further increasing the catalyst dosage to 30 mg leads to a slight decrease in cyclohexanone selectivity to 7.8%. However, an excessive amount of catalyst (e.g., 50 mg) results in a marked decline in the selectivity toward the desired products and promotes the formation of byproducts, negatively affecting the overall reaction performance. Notably, the highest conversion of cyclohexane is also observed at a catalyst dosage of 10 mg, indicating it as the optimal amount for this system. Fig. 4b evaluates the influence of H_2O_2 as the oxidant. In the absence of H_2O_2, no reaction occurs. The addition of H_2O_2 significantly enhances catalytic activity, with the best performance observed when the molar ratio of cyclohexane to H_2O_2 is 1∶4, yielding a cyclohexane conversion of 19.3% and total selectivity of 96.7%. Experiments with higher amounts of H_2O_2 are not attempted for safety reasons. Previous studies by Sun et al.[36] have reported that excessive H_2O_2 leads to accumulation of water and inefficient consumption of the oxidant, both of which hinder catalytic efficiency. Fig. 4c explores the effect of different solvents. Acetonitrile (ACN) exhibits excellent performance due to its high polarity and good solubility for both cyclohexane and H_2O_2[37]. ACN can also react with H_2O_2 to generate active intermediates that facilitate the transfer of active oxygen species, thereby enhancing the oxidation efficiency[38]. When comparing various solvents, polar solvents such as N, N-dimethylformamide (DMF) and ACN achieve high AA selectivity (67.8% and 73.3%, respectively). In contrast, solvents with moderate polarity such as EtOAc or Dichloromethane (DCM) yield lower AA selectivity (~ 60%), while the non-polar solvent 1,2-dichloroethane (DCE) shows negligible catalytic activity[39]. These results underscore the critical role of the solvent in promoting the activation and utilization of H_2O_2, with highly polar solvents being more favorable for this oxidation system[40]. The influence of reaction temperature is also investigated (Fig. 4d). At 60 °C, the catalytic efficiency is lowest, with KA oil (a mixture of cyclohexanol and cyclohexanone) as the predominant product. Increasing the temperature accelerates the oxidation rate, promoting the sequential transformation from cyclohexanol to cyclohexanone and eventually to AA, as both alcohol and ketone intermediates are crucial for acid formation[40]. However, further temperature elevation leads to the generation of more byproducts, reducing the overall selectivity. This is likely due to the enhanced occurrence of side reactions at higher temperatures. Consequently, 100 °C is identified as the most suitable reaction temperature, balancing conversion and selectivity.

To evaluate the stability of the catalyst, eight consecutive reaction cycle tests were carried out, with the results shown in Fig. 5a. The conversion of cyclohexane remains stable over the eight cycles, while the selectivity toward acid products decreases from 73.3% to 58.8%, indicating a gradual degradation in catalytic performance during the reaction process. To further investigate the reasons for performance degradation, the spent catalyst was characterized. XRD patterns (Fig. 5b) reveal a deterioration in the crystallinity of the Cu/Cu_2O phase in the used catalyst, which may be the key structural factor responsible for the decreased selectivity toward acid products[41]. This finding also reinforces that the formation of a well-defined Cu/Cu_2O structure is essential for achieving enhanced catalytic performance. However, SEM images (Fig. 5c and Fig. S2) confirm that the overall morphology and the porous structure of the biomass-derived carbon support remained intact after reaction. Therefore, the decline in catalytic performance can only be attributed to the disruption of the Cu/Cu_2O structure, which reduces the synergistic effect between copper and the carbon support, consequently leading to a decrease in active sites[42]. Furthermore, a performance comparison is provided in Fig. S9 between the catalyst developed in this work (Cu/Cu_2O@C-0.1) and various reported catalysts, including carbon-supported Cu, other Cu-based composites, and nanoparticle catalysts. The results demonstrate that Cu/Cu_2O@C-0.1 achieves superior cyclohexane conversion and adipic acid selectivity, underscoring its outstanding catalytic efficacy and potential for practical application.

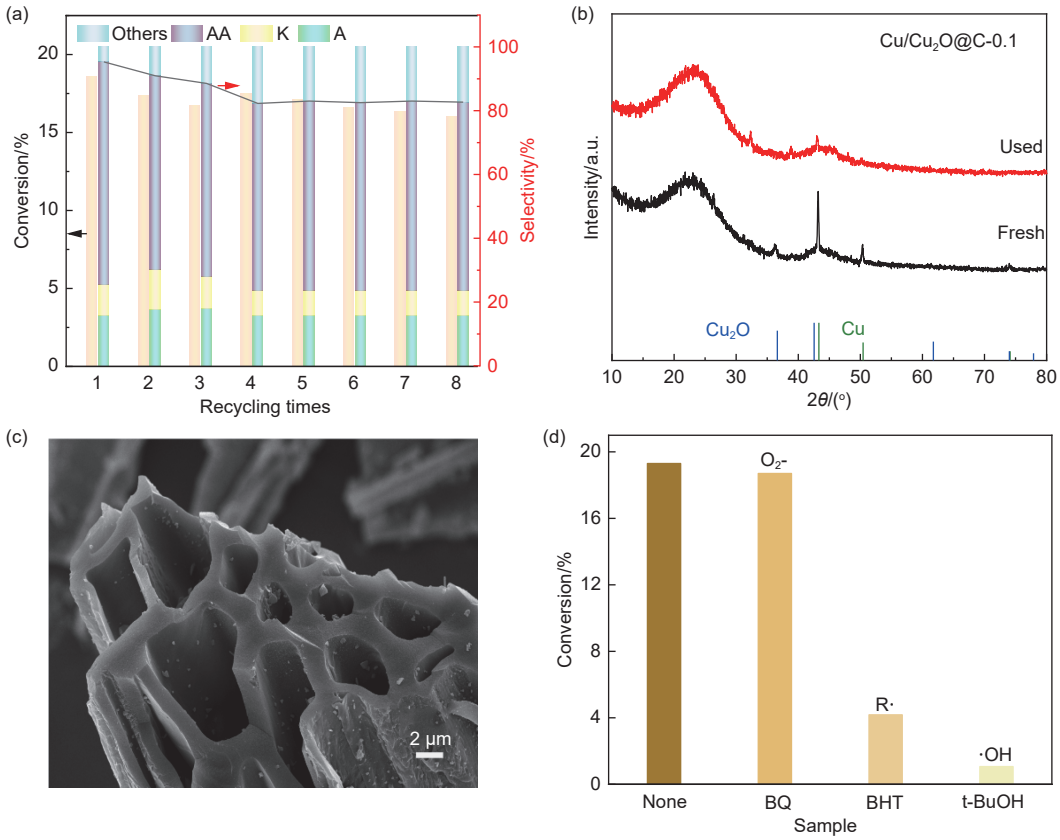

Fig. 5 (a) Recyclability test of catalyst; (b) XRD patterns of fresh and used Cu/Cu_2O@C-0.1. (c) SEM spectra of used Cu/Cu_2O@C-0.1. (d) Effect of different scavengers on cyclohexane reaction catalyzed by Cu/Cu_2O@C-0.1

3.3 The proposed reaction mechanism

Based on relevant literature and experimental results, this study confirms that the catalytic reaction proceeds by a free radical mechanism[43]. As clearly illustrated in Fig. 5d, we systematically investigated the reaction mechanism using 1,4-benzoquinone (BQ), tert-butanol (t-BuOH), and butylated hydroxytoluene (BHT) as specific radical scavengers for superoxide anion radicals (•O_2^-), hydroxyl radicals (•OH), and alkyl radicals (R•), respectively. A slight decrease in the conversion of cyclohexane is observed when BQ is employed as a scavenger, suggesting a limited role of O_2•$^-$ in the reaction. Experimental data reveal that the addition of BHT causes a significant decrease in cyclohexane conversion from 19.3% to 4.18%, demonstrating the essential role of alkyl radicals (R•) as reactive intermediates in the catalytic cycle. Most strikingly, when t-BuOH is introduced into the reaction system, cyclohexane conversion rate plummets to near-negligible levels, providing compelling evidence that hydroxyl radicals (•OH) serve as the primary driving force for the reaction[44]. These comprehensive radical trapping experiments unambiguously demonstrate that the Cu/Cu_2O@C-0.1 catalyzed cyclohexane oxidation follows a free radical chain mechanism, with both hydroxyl radicals (•OH) and alkyl radicals (R•) being indispensable reactive species. This mechanistic understanding, supported by robust experimental evidence, offers valuable insights on designing more efficient catalytic systems for cyclohexane oxidation[45].

Based on systematic characterization analysis and catalytic performance evaluation, combined with current understanding of hydroxyl radical mechanisms in cyclohexane oxidation, this study elucidates the reaction mechanism of cyclohexane selective oxidation mediated by Cu/Cu_2O@C-0.1 catalyst (Fig. 6). The radical chain reaction process involves 4 key steps. Firstly, hydrogen peroxide undergoes homolytic cleavage at the Cu active sites on the catalyst surface, efficiently generating highly reactive hydroxyl radicals (•OH). Secondly, these •OH radicals activate

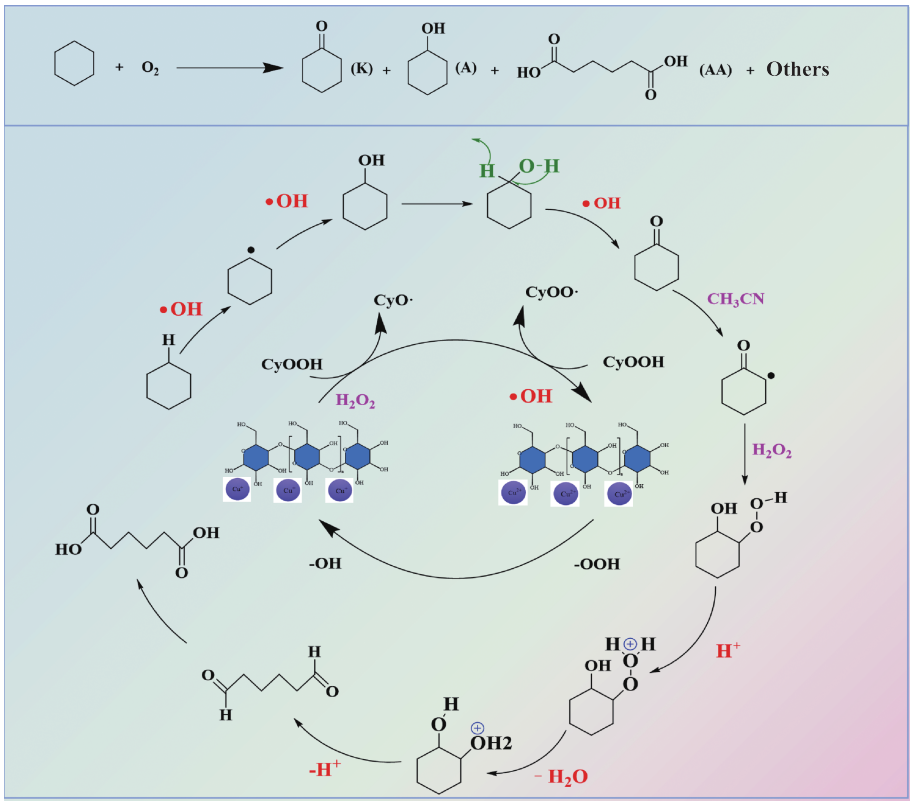

Fig. 6 Possible mechanism of Cu/Cu_2O@C-0.1 catalyzed formation of AA from cyclohexane

cyclohexane molecules through hydrogen abstraction to form crucial cyclohexyl radical intermediates (Cy•). These Cy• radicals then undergo radical coupling with •OH in the solution to selectively produce cyclohexanol. Ultimately, cyclohexanol is converted to cyclohexanone via dehydrogenation oxidation under continuous catalytic action[46].

Notably, the reaction system simultaneously involves radical recombination pathways. Through the formation of 2-hydroxycyclohexanone intermediate and subsequent proton-induced C—C bond cleavage, 1,6-hexanedial intermediate is ultimately formed and further oxidized to yield adipic acid, the target product. This mechanism highlights the critical role of Cu active centers in regulating radical reaction pathways, providing a theoretical foundation for understanding the superior performance of this catalytic system.

4 Conclusion

In conclusion, this study developed a simple and eco-friendly strategy to synthesize biomass-derived carbon-supported copper catalysts for the one-step oxidation of cyclohexane to adipic acid. The results reveal that during carbonization, Cu^{2+} species are reduced to Cu/Cu_2O nanoparticles, which are uniformly anchored onto the carbon support surface with the assistance of inherent defect in the carbon matrix, forming highly dispersed and stable active sites. The optimized Cu/Cu_2O@C-0.1 catalyst achieves a cyclohexane conversion of 19.3% and an adipic acid selectivity of 73.3%. The oxidation reaction catalyzed by Cu/Cu_2O@C-0.1 follows a free radical chain mechanism, in which hydroxyl radicals (•OH) and alkyl radicals (R•) play important roles. These results demonstrate that enhanced catalytic performance is attributed to the Cu/Cu_2O structure and its synergy with the carbon support. This work highlights the potential of biomass carbon as a sustainable catalyst support and provides insights into the design of more efficient and sustainable copper-based oxidation catalysts for industrial applications.

Acknowledgements

This work was supported by the Inner Mongolia Autonomous Region Universities Basic Scientific Re-

search Project (2023QNJS053, 2023CXPT002), the Inner Mongolia Autonomous Region Key R&D and Achievement Transformation Program Projects (2025YFDZ0005), the National Natural Science Foundation (21902080, 42263004, 22406191).

References

[1] Qiu Y H, Hartwig J F. Mechanism of Ni-catalyzed oxidations of unactivated C(sp^3)-H bonds[J]. Journal of the American Chemical Society, 2020, 142(45): 19239-19248.

[2] Abutaleb A, Ali M A. A comprehensive and updated review of studies on the oxidation of cyclohexane to produce ketone-alcohol (KA) oil[J]. Reviews in Chemical Engineering, 2022, 38(7): 769-797.

[3] Acharyya S S, Ghosh S, Bal R. Nanoclusters of Cu(II) supported on nanocrystalline W(VI) oxide: a potential catalyst for single-step conversion of cyclohexane to adipic acid[J]. Green Chemistry, 2015, 17(6): 3490-3499.

[4] Jiang M, Li T, Wei X, et al. Resolving water-induced deactivity and fragility of Prussian blue by eutectic chemistry for upgraded sodium storage[J]. Journal of Energy Chemistry, 2026, 118: 169-177.

[5] Jiang M, Zhao Y, Hou Z, et al. Leveraging sodium storage of water-deficient prussian blue analogues by deep eutectic chemistry[J]. Acs Energy Letters, 2026, 11(1): 526-536.

[6] Mazzi A, Paul S, Cavani F, et al. Cyclohexane oxidation to adipic acid under green conditions: A scalable and sustainable process[J]. Chemistry Catalysis Chemistry, 2018, 10(17): 3680-3682.

[7] Chen L, Zhou Y, Gui Z, et al. Au nanoparticles confined in hybrid shells of silica nanospheres for solvent-free aerobic cyclohexane oxidation[J]. Journal of Materials Science, 2017, 52(12): 7186-7198.

[8] Alshammari A, Kalevaru V N, Martin A. Bimetallic catalysts containing gold and palladium for environmentally important reactions[J]. Catalysts, 2016, 6(7): 97.

[9] Alnefaie R S, Abboud M, Alhanash A, et al. Efficient oxidation of cyclohexane over bulk nickel oxide under mild conditions[J]. Molecules, 2022, 27(10): 3145.

[10] Kvande K, Garetto B, Deplano G, et al. Understanding C-H activation in light alkanes over Cu-MOR zeolites by coupling advanced spectroscopy and temperature-programmed reduction experiments[J]. Chemical Science, 2023, 14(36): 9704-9723.

[11] Wittmann C, Palamarciuc O, Dascalu M, et al. Copper(ii) complex with a redox-noninnocent Schiff base bearing a tetraphenyldisiloxane unit: synthesis, structure and catalytic oxidation of cyclohexane[J]. Dalton Transactions, 2025, 54(28): 10984-11005.

[12] Liu J K, Yang H, Kara U I, et al. A facile synthesis of stable copper-based core-shell catalysts for highly efficient 4-nitrophenol reduction and benzyl alcohol oxidation[J]. Chemical Engineering Journal, 2024, 479: 147778.

[13] Shahzeydi A, Ghiaci M, Farrokhpour H, et al. Facile and green synthesis of copper nanoparticles loaded on the amorphous carbon nitride for the oxidation of cyclohexane[J]. Chemical Engineering Journal, 2019, 370: 1310-1321.

[14] Zhu G, Chen L, Lu T, et al. Cu-based MOF-derived architecture with Cu/Cu_2O nanospheres anchored on porous carbon nanosheets for efficient capacitive deionization[J]. Environmental Research, 2022, 210: 112909.

[15] Andrade M A, Mestre A S, Carvalho A P, et al. The role of nanoporous carbon materials in catalytic cyclohexane oxidation[J]. Catalysis Today, 2020, 357: 46-55.

[16] Xie C J, Xiong Q, Jiang L, et al. Carbon supported copper catalyst prepared in situ by one-pot pyrolysis of Bougainvillea glabra: An efficient and stable catalyst for selective oxidation of cyclohexane[J]. Applied Surface Science, 2022, 576: 151833.

[17] Zhou H L, Guo C, Zhou S Q, et al. Cyanobacterial hydrothermal carbonization carbon as photocatalyst for selective aerobic oxidation of cyclohexane[J]. Journal of Environmental Chemical Engineering, 2024, 12(6): 114487.

[18] Huang H M, Lan Z W, Li W J, et al. A novel and low-cost CuPc@C catalyst derived from the compounds of sunflower straw and copper phthalocyanine pigment for oxygen reduction reaction[J]. Royal Society of Chemistry Advances, 2021, 11(26): 15590-15597.

[19] Gawlig C, Schindler S, Becker S. One - pot conversion of cyclohexane to adipic acid using a μ4 - oxido - copper cluster as catalyst together with hydrogen peroxide[J]. European Journal of Inorganic Chemistry, 2019, 2020(3): 248-252.

[20] Graça I, Chadwick D. NH_4-exchanged zeolites: Unexpected catalysts for cyclohexane selective oxidation[J]. Microporous and Mesoporous Materials, 2020, 294: 109873.

[21] Khataee A, Kalderis D, Gholami P, et al. Cu_2O-CuO@biochar composite: Synthesis, characterization and its efficient photocatalytic performance[J]. Applied Surface Science, 2019, 498: 143846.

[22] Jian J, You K, Duan X, et al. Boosting one-step conversion of cyclohexane to adipic acid by NO_2 and VPO composite catalysts[J]. Chemical Communications, 2016, 52(16): 3320-3323.

[23] Kuznetsov M, Pombeiro A. Metal-free and iron(II)-assisted oxidation of cyclohexane to adipic acid with ozone: A theoretical mechanistic study[J]. Journal of Catalysis, 2021, 399: 52-66.

[24] Li Y W, Li H, Li K X, et al. Roles of oxygen vacancies in CeO_2 nanostructures for catalytic aerobic cyclohexane oxidation[J]. American Chemical Society Applied Nano Materials, 2023, 6(15): 14214-14227.

[25] Liang F, Zhong W, Xiang L, et al. Synergistic hydrogen atom transfer with the active role of solvent: Preferred one-step aerobic oxidation of cyclohexane to adipic acid by N-hydroxyphthalimide[J]. Journal of Catalysis, 2019, 378: 256-269.

[26] Yang K, Yan Y, Wang H, et al. Monodisperse Cu/Cu_2O@C core-shell nanocomposite supported on rGO layers as an efficient catalyst derived from a Cu-based MOF/GO structure[J]. Nanoscale, 2018, 10(37): 17647-17655.

[27] Librando I L, Paul A, Mahmoud A G, et al. Triazaphosphaadamantane-functionalized terpyridine metal complexes: cyclohexane oxidation in homogeneous and carbon-supported catalysis[J]. RSC Sustainability, 2023, 1(1): 147-158.

[28] Liu X, Conte M, Sankar M, et al. Liquid phase oxidation of cyclohexane using bimetallic Au–Pd/MgO catalysts[J]. Applied Catalysis A: General, 2015, 504: 373-380.

[29] Zhang G, Yan J, Wang J, et al. Effect of carbon support on the catalytic performance of Cu-based nanoparticles for oxidative carbonylation of methanol[J]. Applied Surface Science, 2018, 455: 696-704.

[30] Nobbs J, Zainal N, Tan J, et al. Bio-based pentenoic acids as intermediates to higher value-added mono- and dicarboxylic acids[J]. ChemistrySelect, 2016, 1(3): 539-544.

[31] Park M, Kim B, Kim S, et al. Improved binding between copper and carbon nanotubes in a composite using oxygen-containing functional groups[J]. Carbon, 2011, 49(3): 811-818.

[32] Xu M D, Yu Y L, Shi G J, et al. Curved surface of graphitic carbon nitride boosting cyclohexane oxidation over single-atom catalysts[J]. American Chemical Society Applied Nano Materials, 2024, 7(10): 11952-11964.

[33] Yousefzadeh H, Bozbag S E, Sushkevich V, et al. Stepwise conversion of methane to methanol over Cu-mordenite prepared by supercritical and aqueous ion exchange routes and quantification of active Cu species by H_2-TPR[J]. Catalysis Communications, 2023, 174: 106574.

[34] Bi D M, Yin M Q, Huang F P, et al. Evolution and prediction model of environmentally-persistent free radicals in biomass three-component pyrolytic carbon with pyrolysis temperature[J]. Industrial Crops and Products, 2023, 206: 117643.

[35] Muthukumar P, Kumar V V, Reddy G R K, et al. Fabrication of strong bifunctional electrocatalytically active hybrid Cu-Cu_2O nanoparticles in a carbon matrix[J]. Catalysis Science & Technology, 2018, 8(5): 1414-1422.

[36] Sun L, Liu J, Luo W, et al. Preparation of amorphous copper - chromium oxides catalysts for selective oxidation of cyclohexane[J]. Molecular Catalysis, 2018, 460: 16-26.

[37] Sadiq M, Khan M, Numan M, et al. Tuning of activated carbon for solvent-free oxidation of cyclohexane[J]. Journal of Chemistry, 2017, 2017: 5732761.

[38] Guo Y, Ying T, Liu X, et al. A partially graphitic carbon catalyst for aerobic oxidation of cyclohexane[J]. Molecular Catalysis, 2019, 479: 170-175.

[39] Spassova I, Stoeva N, Nickolov R, et al. Impact of carbon on the surface and activity of silica-carbon supported copper catalysts for reduction of nitrogen oxides[J]. Applied Surface Science, 2016, 369: 120-129.

[40] Yadav V K, Shinde H P, Das T. Oxidation of cyclohexane using copper-nickel catalyst[J]. Arabian Journal for Science and Engineering, 2021, 47(5): 5601-5612.

[41] Zheng A, Zhou Q, Ding B, et al. Reduced amino acid schiff base-iron(III) complexes catalyzing oxidation of cyclohexane with hydrogen peroxide[J]. European Journal of Inorganic Chemistry, 2021, 2021(33): 3385-3395.

[42] Xie C J, Wang W, Yang Y P, et al. Enhanced stability and activity for solvent-free selective oxidation of cyclohexane over Cu_2O/CuO fabricated by facile alkali etching method[J]. Molecular Catalysis, 2020, 495: 111134.

[43] Liu Y M, Yang D S, Zeng G X, et al. Highly efficient one-pot aerobic oxidation of cyclohexane to adipic acid using task-specific metal-based ionic liquid[J]. Chemical Engineering Science, 2024, 283: 119373.

[44] Yuan E X, Zhou M X, Jian P M, et al. Atomically dispersed Co/C_3N_4 for boosting aerobic cyclohexane oxidation[J]. Applied Surface Science, 2023, 613: 155886.

[45] Zuhra Z, Abbas Y, Ali S, et al. Fe_3O_4@MOF hybrid for supercilious recovery of Au(III) and Pd(II) from e-waste and spent as catalysts for cyclohexane oxidation[J]. Journal of Cleaner Production, 2023, 404: 136966.

[46] Makgwane P, Ray S. Efficient room temperature oxidation of cyclohexane over highly active hetero-mixed WO_3/V_2O_5 oxide catalyst[J]. Catalysis Communications, 2014, 54: 118-123.